Journal of Biomolecular Structure and Dynamics

ISSN: (Print) (Online) Journal homepage: https://www.tandfonline.com/loi/tbsd20

Targeting Olokizumab-Interleukin 6 interaction interface to discover novel IL-6 inhibitors

Que-Huong Tran, Hoang-Nhi Cao, Dac-Nhan Nguyen, Thi-Thuy-Nga Tran, Minh-Tri Le, Quoc-Thai Nguyen, Van-Thanh Tran, Viet-Hung Tran & Khac-Minh Thai

To cite this article: Que-Huong Tran, Hoang-Nhi Cao, Dac-Nhan Nguyen, Thi-Thuy-Nga Tran, Minh-Tri Le, Quoc-Thai Nguyen, Van-Thanh Tran, Viet-Hung Tran & Khac-Minh Thai (2023): Targeting Olokizumab-Interleukin 6 interaction interface to discover novel IL-6 inhibitors, Journal of Biomolecular Structure and Dynamics, DOI: 10.1080/07391102.2023.2193990

To link to this article: https://doi.org/10.1080/07391102.2023.2193990

JOURNAL OF BIOMOLECULAR STRUCTURE AND DYNAMICS
https://doi.org/10.1080/07391102.2023.2193990

Targeting Olokizumab-Interleukin 6 interaction interface to discover novel IL-6 inhibitors

Que-Huong Tran[a,b], Hoang-Nhi Cao[a], Dac-Nhan Nguyen[a], Thi-Thuy-Nga Tran[a,b], Minh-Tri Le[a,c], Quoc-Thai Nguyen[a], Van-Thanh Tran[a], Viet-Hung Tran[d,e] and Khac-Minh Thai[a]

[a]Faculty of Pharmacy, University of Medicine and Pharmacy at Ho Chi Minh City, Ho Chi Minh City, Vietnam; [b]Department of Pharmaceutical Chemistry, Da Nang University of Medical Technology and Pharmacy, Da Nang, Vietnam; [c]School of Medicine, Vietnam National University Ho Chi Minh City, Ho Chi Minh City, Vietnam; [d]Faculty of Traditional Medicine, University of Medicine and Pharmacy at Ho Chi Minh City, Vietnam; [e]Institute of Drug Quality Control Ho Chi Minh City, Ho Chi Minh City, Vietnam

Communicated by Ramaswamy H. Sarma

ABSTRACT

The IL-6/IL-6R or IL-6/GP130 protein-protein interactions play a significant role in controlling the development of chronic inflammatory diseases, such as rheumatoid arthritis, Castleman disease, psoriasis, and, most recently, COVID-19. Modulating or antagonizing protein-protein interactions of IL6 binding to its receptors by oral drugs promises similar efficacy to biological therapy in patients, namely monoclonal antibodies. In this study, we used a crystal structure of the Fab part of olokizumab in a complex with IL-6 (PDB ID: 4CNI) to uncover starting points for small molecule IL-6 antagonist discovery. Firstly, a structure-based pharmacophore model of the protein active site cavity was generated to identify possible candidates, followed by virtual screening with a significant database Drugbank. After the docking protocol validation, a virtual screening by molecular docking was carried out and a total of 11 top hits were reported. Detailed analysis of the best scoring molecules was performed with ADME/T analysis and molecular dynamics simulation. Furthermore, the Molecular Mechanics-Generalized Born Surface Area (MM/GBSA) technique has been utilized to evaluate the free binding energy. Based on the finding, one newly obtained compound in this study, namely DB15187, may serve as a lead compound for the discovery of IL-6 inhibitors.

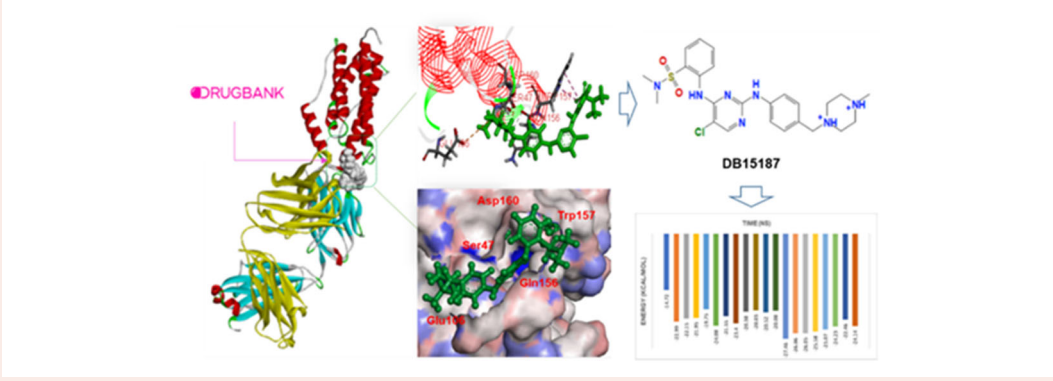

ARTICLE HISTORY
Received 5 October 2022
Accepted 29 January 2023

KEYWORDS
Interleukin 6; protein-protein interaction inhibitors; pharmacophore modeling; molecular docking; molecular dynamic simulation

Introduction

Interleukin-6 (IL-6) is a significant immune system regulator and has been shown to be closely related to autoimmune disease. Under the regulation of chemokines, IL-6 induces increased trafficking of leukocytes, leading to T and B cell proliferation and differentiation (Shaw et al., 2014; Eto et al., 2011). The overproduction of serum IL-6 levels is believed to be responsible for several diseases, such as multiple myeloma, rheumatoid arthritis, Castleman disease, psoriasis, postmenopausal osteoporosis, and, most recently, COVID-19 (Kuhn et al., 2014; Potere et al., 2021). IL-6 stimulates the growth or differentiation of a variety of cells via a receptor system that includes an IL-6 receptor-binding chain (IL-6R) and a shared signaling subunit (glycoprotein 130–gp130) to form a hexameric signaling complex (Choi et al., 2016). In the hexameric complex, the D helix and the A-B ring (site I) of IL-6 bind to the D3 domain of IL-6R. Then, at site II (helices A and C of IL-6), the IL-6/IL-6R complex interacts with gp130 to create a heterotrimer complex. Finally, site III is formed by the

CONTACT Khac-Minh Thai thaikhacminh@ump.edu.vn, thaikhacminh@gmail.com; Viet-Hung Tran tran.viethung168@gmail.com Faculty of Pharmacy, University of Medicine and Pharmacy at Ho Chi Minh City, Ho Chi Minh City, Vietnam

Supplemental data for this article can be accessed online at https://doi.org/10.1080/07391102.2023.2193990.

immunoglobulin-like D1 domain of gp130 with IL-6 (site IIIa) and the D2 domain of IL-6Rα (site IIIb) (Boulanger et al., 2003; Paonessa et al., 1995). The full hexameric complex is required for effective IL-6 signaling, and signaling would not be possible without these three factors.

IL-6 utilizes two pathways to mediate its biological effects: the classical (cis) signaling pathway and the trans-signaling pathway (Akbari & Hassan-Zadeh, 2018). In the classical signaling pathway, IL-6 binds to mIL-6R and significantly promotes anti-inflammatory responses. While by binding to soluble IL6R (sIL6R) complex, IL-6 initiates trans-signaling and induces pro-inflammatory (Pullamsetti et al., 2018; Azevedo et al., 2011). Both cis and trans-signaling must form complexes with the signal transduction co-receptor glycoprotein 130 (gp130) (Lacroix et al., 2015). Dimerization of IL-6/IL-6R/gp130 leads to the initiation of intracellular signaling, through Janus Kinase-Signal Transducer and Activator of Transcription (JAK-STAT), phosphatidylinositol 3-kinase/Akt kinase (PI3-K/AKT) pathways and consequently activate the expression of different genes with crucial roles in inflammation and cancer development (Azevedo et al., 2011; Hirano, 2021).

Potential therapies exist that involve monoclonal antibodies (mAbs) directed against the interface of IL6 and IL-6R or IL-6 and gp130 (Allegra et al., 2013). For example, tocilizumab targeting the IL-6R, blocks the binding of IL-6 to IL-6R at the binding site I, whereas olokizumab targeting the IL6, locks hexamer formation at the binding site IIIa (Karkhur et al., 2019). In addition, there are several mAbs capable of inhibiting IL-6 activity that is being studied in clinical stages such as siltuximab, sarilumab, sirukumab, and clazakizumab (Rose-John et al., 2017). However, mAbs are large proteins that require injection and are therefore not convenient for the patient. In addition, using mAbs also has some disadvantages such as high treatment costs, easy infection, neutropenia, thrombocytopenia, polycythemia vera, and elevated liver enzymes (Castelli et al., 2019). Compared to biological therapeutic agents, small molecule treatment offers many benefits, such as simpler administration, variable pharmacokinetics, and low production costs (Tran et al., 2022). The most important issue in the search for small molecules capable of inhibiting IL-6 activity is determining the co-crystallization crystal structure with suitable resolution containing the active site of IL-6. Fortunately, the crystal structure of the Fab part of olokizumab in complex with IL-6 (PDB ID: 4CNI, resolution: 2.2 Å), which block the interaction between IL-6 and gp130, was determined in 2014 (Shaw et al., 2014; The Protein Data Bank, 2022). It sheds more light on the interaction between IL-6 and its inhibitor at site IIIa.

The identification of small molecules targeting IL-6 could potentially open up new avenues for the discovery of novel therapeutics for the treatment of pathological diseases associated with IL-6 bioactivity. This study focused on small molecules screening for IL-6 inhibitors from the Drugbank database based on the crystal structure of the IL-6/Olokizumab complex.We have applied a suitable in silico approach, including structure-based 3D-pharmacophore models, docking procedures, and molecular dynamic simulations. Besides, the ADME/T analysis is utilized to evaluate the oral bioavailability of top compounds.

Materials and methods

Database set

A database containing 9,213 compounds from the Drugbank database (Wishart et al., 2018) was imported into MOE 2015.10 software (Molecular Operating Environment (MOE),), 2015) to convert them into 3D molecules. In addition, hydrogen atoms are added, partial charges are calculated, and multiple structures per molecule are generated. The configuration limit is set to 10,000, the random search repeat limit is 1,000, the energy minimization repeat limit is 1,000, the energy reduction gradient test is 0.0001, and the input filters will clear. The output formats have been saved as MOE database (*.mdb).

3D-Pharmacophore generation

A high-resolution complex structure of IL-6 in complex with olokizumab monoclonal antibody (pdb id: 4CNI, resolution: 2.2 Å) from Protein Data Bank (PDB) is selected to determine the pharmacophore model on the IIIa active site (The Protein Data Bank, 2022). The crystal structure of olokizumab in complex with IL-6 strongly suggests that olokizumab's mode of action involves maximal blockade of the interaction between IL-6 and gp-130 (site IIIa) (Shaw et al., 2014). The epitope of olokizumab lies in the gp130-binding region of IL-6. Trp157 residue of IL-6 is a critical mediator of the IL-6:gp130, making extensive hydrophobic contacts and hydrogen bonds with tyrosine (Tyr103, and Tyr104) and phenylalanine (Phe33) side chains from the heavy chain of the antibody (Allen & Lumb, 2020). At the interface between IL-6 and olokizumab, residue Gln156 protrudes from the surface of IL-6 into a pocket formed by the CDRs of the antibody. In particular, Gln156 forms hydrophobic interactions with many heavy chain amino acids including Tyr56, Ser102, Phe33, Glu101, and Tyr103 (Verma et al., 2016). The light chain of Olokizumab interacts with IL-6 at two critical amino acids, Leu57 and Asn60 (Shaw et al., 2014). In addition, according to IL-6/Olokizumab interaction analyzed by MOE software, Trp157, Asp160, and Gln156 of IL-6 interact mainly with Phe33, Tyr103, Tyr104, and Tyr 56 amino acids of the HDR of olokizumab, whereas the residues of LDR, including Gly30, Ile31, Asp28, Ala94, and Tyr96 forms hydrophobic interactions and hydrogen bondings with Leu57, Asn60, Ala153, and Asn155 of IL-6. Previous studies have shown that the mutation of Trp157 and Asp 160 would result in a 2-4-fold decrease in the ability to bind and activate the hemaxic complex (Paonessa et al., 1995). Therefore, the features of the 3D-pharmacophore models built based on the chemical features of these residues and spatially favorable locations of their functional groups are perfectly consistent (Figure 1; Table S1) (Thai et al., 2013; Le et al., 2020; Le et al., 2021; Tran et al., 2022; Tran et al., 2022). The pharmacophore query editor tool in MOE 2015.10 software is used to perform this process.

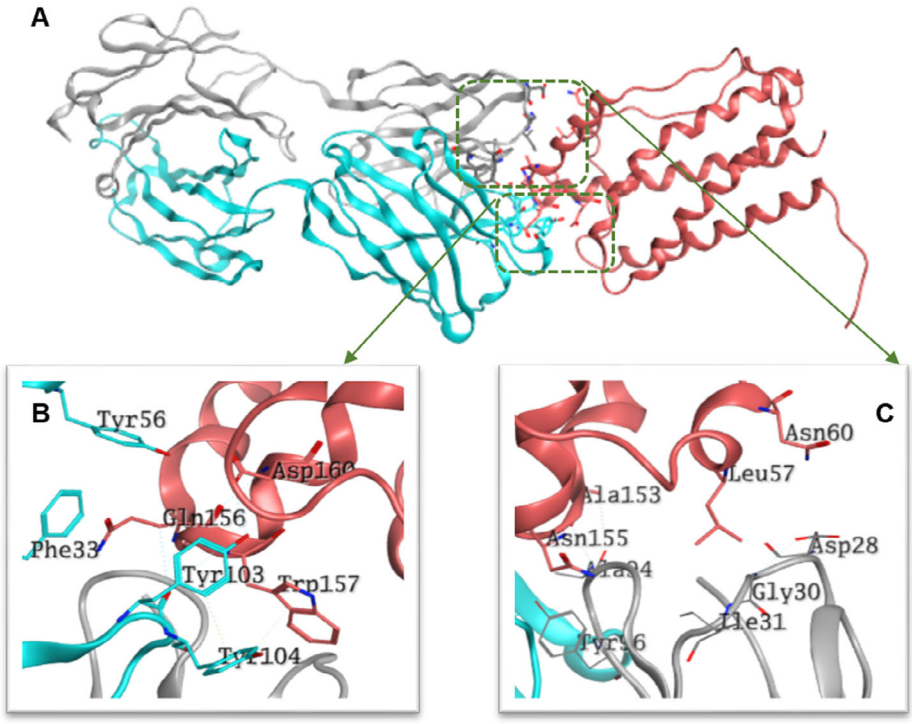

Figure 1. Protein-protein interactions between IL-6 and the antibody Olokizumab. (A) X-ray structure of Olokizumab/IL-6 complex (PDB ID: 4CNI) and the binding site positions. (B) and (C) Isolated critical residues on the binding interface of IL-6 (red) and heavy chain (cyan) and light chain (grey) of Olokizumab.

Table 1. The docking scores of 11 top ligands and their interactions with IL-6.

No	Ligands ID	Docking score (kJ.mol^{-1})	Residues interaction	Satisfying of pharmacophore model
1	DB00619	−25.16	Gln156, Tryp157, Asp160	Ph_2
2	DB06364	−24.20	Gln156, Tryp157, Asp160	Ph_1
3	DB11526	−22.81	Asn155, Tryp157, Asp160	Ph_1
4	DB15187	−22.05	Gln156, Tryp157, Asp160	Ph_1, Ph_2
5	DB06190	−21.71	Gln156, Tryp157, Asp160	Ph_2
6	DB04379	−21.50	Gln156, Tryp157, Asp160	Ph_2
7	DB09079	−21.11	Gln156, Tryp157, Asp160	Ph_2
8	DB16236	−20.67	Gln156, Tryp157, Asp160	Ph_2
9	DB13060	−20.44	Gln156, Tryp157, Asp160	Ph_2
10	DB04125	−20.39	Gln156, Tryp157, Asp160	Ph_2
11	DB07601	−20.03	Gln156, Tryp157, Asp160	Ph_2

Molecular docking

Protein preparation

IL-6/Olokizumab complex (pdb id: 4CNI) was imported in MOE 2015.10 after being collected from the Protein Drug Bank. Unrelated protein sequences were removed and only the C sequence of the IL-6 structure was retained for the docking procedure. Protein was then prepared using the QuickPrep tool in MOE (Molecular Operating Environment (MOE),), 2015), including protonating and charging amino acids (protonate), minimizing energy (tether and minimize), and converting *.pdb format.

Ligands prepare

The ligand databases were energy minimized by using MOE 2015.10 software with Amber10: EHT force field (Case et al., 2005). The results were converted and saved as a *.sdf format suitable for the docking software.

Docking model

Identifying the location of protein binding sites helps generate enough contact points with the protein and significantly increases docking efficiency. This study used the FlexX tool of BioSolveIT LeadIT 2.1.8 software (LeadIT 2.1.8, 2.1.8, 2022) to attach ligands to specific amino acid positions in the protein binding pocket and evaluate this association. In FlexX, a binding pocket was defined by selecting the residues of the protein (grid points) within10 Å radius from the ligand atom. Based on energy values, the top ranked poses for each ligand in the data set were selected for further analysis (Kontoyianni et al., 2004). Regarding that, the seven-crucial residues found in the IL-6 protein at the binding site, including Leu57, Asn60, Ala153, Asn155, Gln156, Tryp157, and Asp160 are loaded into the LeadIT software and expanded with a suitable radius (10 Å). Subsequently, the prepared ligands were imported into the LeadIT software to be docked into the protein. The docking process used the following parameters: the maximum number of solutions per iteration

was 1000, that per fragmentation was 200, the number of poses to keep was the top 10, and default docking options were used (Ngo et al., 2016). The docking process had been completed, and well-bound ligands were ranked based on the docking score ($kJ.mol^{-1}$). Moreover, the Protein-Ligand Interaction Fingerprinting (PLIF) tool of the MOE 2015.10 software (Molecular Operating Environment (MOE),), 2015) was used to analyze the interaction patterns between the ligands with the crucial residues at the binding pocket. Accordingly, the interactions in PLIF are classified into six types: side chain hydrogen donor (D), side chain hydrogen bond acceptor (A), backbone hydrogen bond donor (d), bond acceptor backbone hydrogen bond (a), ionic attraction (I), arene-arene interaction (R) and surface contact (C) (Sekhar Pagadala, 2021).

ADME and toxicity test

ADME

ADME is important to analyze the pharmacodynamics of the proposed molecule which could be used as a drug. The SwissADME online free tool (http://www.swissadme.ch/, accessed on 8 August 2022) was employed for this study to evaluate the individual ADME behavior like physiochemical properties, pharmacokinetics, drug-likeness, and medicinal chemistry properties of the compounds. The best ligands after molecular connection were uploaded directly to the submission page (http://www.swissadme.ch) in *.smlie format. The results are presented for each molecule in tables, graphs, and also an excel spreadsheet (Daina et al., 2017).

Toxicity test

Calculation-based methods have made it possible to obtain a safety profile of the desired compound to measure toxicity through computational methods. The toxicity risk model is provided by ADMET Predictor 10.3 software (Simulations Plus, 2022). Toxicity risk value (TOX Risk) ≤ 2, larger numbers indicate molecules are less likely to pass preclinical and clinical trials (Wang, 2009).

Molecular dynamics simulations

To evaluate the stability over time, the compound with the highest binding energy for the protein target is simulated by MD simulation to check the stability of the compound in the binding pocket. Then, GROMACS, 2021.2 software package (Ngo et al., 2016; GROMACS, 2021) was used to simulate the molecular dynamics of the apoprotein and protein-ligand complexes for 50 ns and 200 ns, respectively. Protein topology was prepared by the pdb2gmx module of GROMACS using the all-atom CHARMM27 force field (Brooks et al., 2009). The Avogadro software (Hanwell et al., 2012) was used to add hydrogen atoms to the ligands before generating their topology by the SwissParam online tool (Zoete et al., 2011). To ensure the total charge neutrality of the simulated system, a corresponding number of sodium ions was added to replace the water molecules in the three systems to produce a dodecahedron solvent box of the appropriate size. Finally, the system was equilibrated and separated into two phases to minimize excessive protein distortion during MD. Phase 1 - NVT (particle constant, volume, temperature) with temperature parameters of 300 K and setup time of 100 ps. Phase 2 - NPT (particle constant, pressure, temperature) at 0.987 atm and 100 ps setup time.

The protein stability in free (apoprotein) and complex forms was evaluated using the MD simulation trajectories to calculate the relevant values. The protein structure is considered stable and significant during dynamic simulation when the RMSD (Root Mean Square Deviation) and RMSF (Root Mean Square Fluctuation) fluctuations are less than 0.2 nm. The ability to retain the spatial structure of the protein during simulation is presented throughout gyration radius (Rg) and the solvent accessible surface area (SASA) values. By using VMD 1.9.4 software, hydrogen bond formation was examined to determine the ability of the ligand to interact with the major residues. A hydrogen bond was defined by geometric criteria, including a distance between hydrogen donor (D) and acceptor (A) atoms of <3.5 Å and an angle of D–H … A $> 120^{\circ}$ (Humphrey et al., 1996).

Binding free energy

From the MD trajectories, the Molecular Mechanics-Generalized Born Surface Area (MM/GBSA) approach was used to determine the binding free energy (Valdés-Tresanco et al., 2021). The binding free energy (ΔE_{bind}) was evaluated determined according to the following equations (Wang et al., 2019):

$$\Delta E_{bind} = E_{complex} - (E_{receptor} + E_{ligand})$$
$$\Delta E_{bind} = \Delta E_{gas} + \Delta E_{sol} - T\Delta S$$
$$\Delta E_{gas} = \Delta E_{ele} + \Delta E_{vdw}$$
$$\Delta E_{sol} = \Delta E_{GB} + \Delta E_{SA}$$

Where $E_{complex}$ is the free energy of the protein-ligand complex, $E_{receptor}$, and E_{ligand} are the free energies in the solution of the isolated protein and ligand, respectively. ΔE_{gas} represents the gas phase interaction energy between the protein and the ligand, which includes electrostatic interaction energies (ΔE_{ele}), van der Waals (ΔE_{vdw}), and internal energies. ΔE_{sol} is the free energy of solvation estimated as the sum of the polar free energy of solvation (ΔE_{GB}) calculated with the generalized born model and the non-polar free energy of solvation (ΔE_{SA}) obtained by fitting SASA. $T\Delta S$ presents the entropy changes estimated by a normal mode analysis on a set of conformational snapshots during the molecular dynamics process. Nevertheless, several researchers have reported that the lack of entropy evaluation is not critical for calculating MM/GBSA binding free energies for protein-ligand complexes (Genheden & Ryde, 2015). For this reason, the entropy contribution $T\Delta S$ of all complexes was not calculated.

Results and discussions

Generation of structure-based reference pharmacophore models

3D pharmacophore modeling is a powerful tool to encode a ligand's physicochemical properties in space, which are

supposed to be important for ligand-target binding. Such a model can be used for virtual screening for novel ligands matching the pharmacophore features. In this study, we used interaction modes between IL-6 protein and olokizumab antibody to generate structure-based pharmacophore models. Since the interactive region is too large, two pharmacophore models have been designed at the respective sites. These models had a suitable number of pharmacophore points and spatial distance for small molecule screening.

On the first binding site (site I), the pharmacophore model including five features was constructed from the H-Olokizumab antibody's residues interacted with the site III epitope (N-terminal region of D helix) of IL-6 (Shaw et al., 2014). Four of them were hydrophobic, and one was a hydrogen acceptor. In detail, the Phe33, Tyr 103, Tyr104, and Tyr56 residues of HC CDR1 formed a network of hydrophobic interactions with Trp157 and Gln156 residues in the helix-D of IL-6. Besides, a hydrogen bond was established between Asp160 of IL6 and Tyr103 of H-Olokizumab. In that way, the first pharmacophore model (Ph-1) was generated as follows: Tyr103 (F1: Hyd, F2: Acc), Tyr104 (F3: Hyd), Phe33 (F4: Hyd), Tyr56 (F5: Hyd) (Figure 2A).

The second pharmacophore model (Ph-2) also comprised five features at the binding site II. Particularly, while the carbonyl group of Asp28 in the L-Olokizumab accepted a hydrogen bond from the amid backbone of Asn60 in the A/B loop of IL-6 (Shaw et al., 2014), one donor hydrogen bond was formed with the oxygen atom of Ala153 and the amine group of Ala94. Additionally, Gly30, Ile31, and Tyr96 of the LC CDR1 loop joined the hydrophobic interaction with the hydrophobic residues Leu57 and Asn155. Hence, this model includes 5 features: Gly30 (F1: Hyd), Ile31 (F2: Hyd), Asp28 (F3: Acc), Tyr96 (F4: Hyd), Ala94 (F5: Don) (Figure 2B).

A database of more than 5 million conformations of the Drugbank library was virtually screened by two pharmacophore models, in which 323 compounds satisfied the models, with 137 structures from the Ph-1 model and 186 structures from the Ph-2 model. These substances were docked into the binding site of IL-6 on the next step.

Docking study

As to structure-based drug design, molecular docking is a widely used method to model interactions and evaluate binding affinity between a small molecule and a protein. Therefore, a molecular docking simulation was performed in this study to elucidate the binding mode of the ligand-receptor. The compounds that satisfied the 3D-pharmacophore models previously have been docked to the binding pocket of IL-6. Among 323 substances docked into IL-6 protein, the success rate was 97.8% (316 structures), while only 7 chemicals could not be docked into the protein. Regarding docking score, there was 81% of substances had a negative result, meaning these compounds are predicted to well contacted with the protein. Specifically, eleven substances gained strong interaction with the docking score of under $-20\,kJ.mol^{-1}$ and were considered top hits. The top eleven ligands bound neatly to the designated binding pocket on IL-6 were illustrated in Figure 3, and their docking score were shown in Table 1.

Furthermore, the interaction occupancy of different ligand conformations in the binding pocket was analyzed throughout the protein-ligand interaction fingerprint by using the PLIF tool

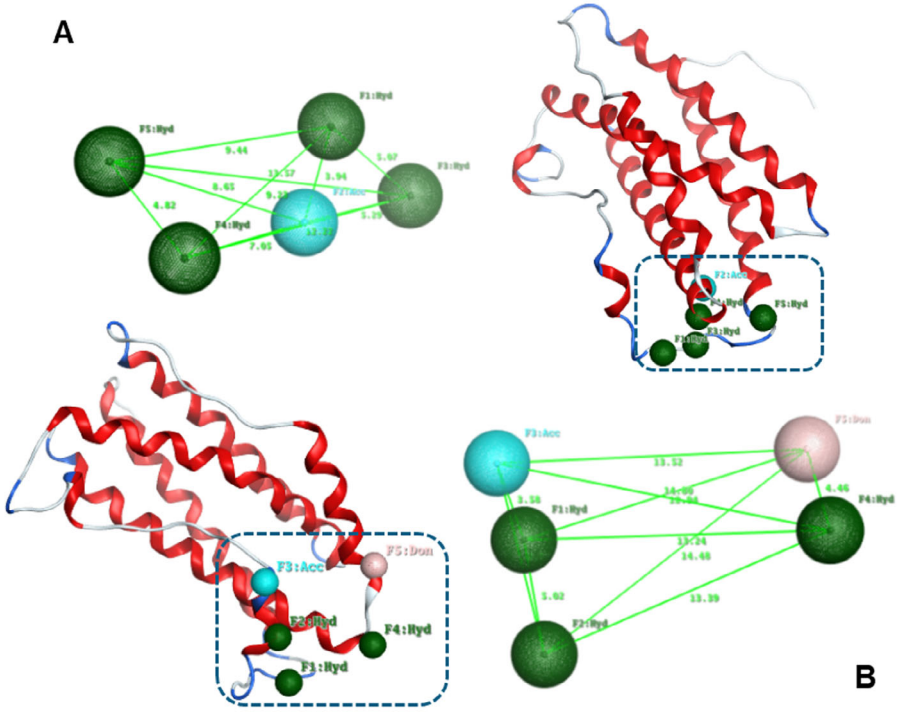

Figure 2. Two 3D-pharmacophore models and their alignment to the IL-6 backbone at site I (Ph-1, A) and site II (Ph-2, B). Each sphere represents an abbreviated pharmacophore feature: Don (light pink), Acc (cyan), and Hyd (dark green). The light green presented the distance (Ð) between pharmacophore points.

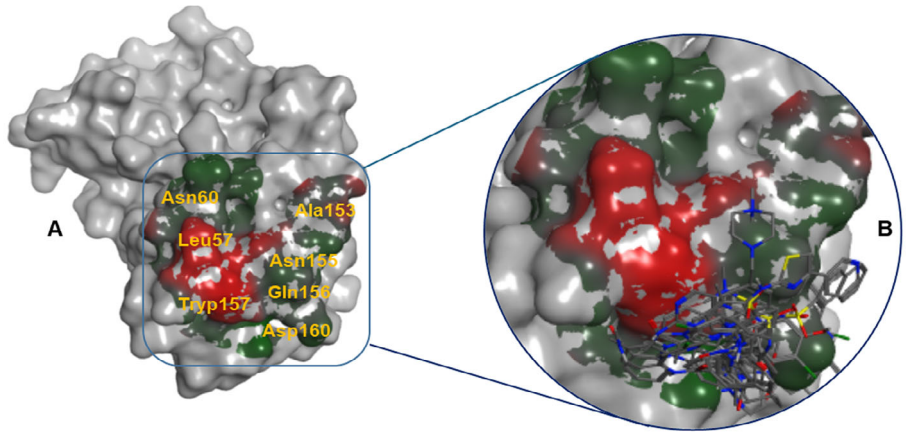

Figure 3. Molecular docking results. (A) The molecular docking model was in the green and red region, and the remaining residues of IL-6 were in grey, (B) Binding poses of the top ten ligands (dark grey) in the IL-6 binding pocket.

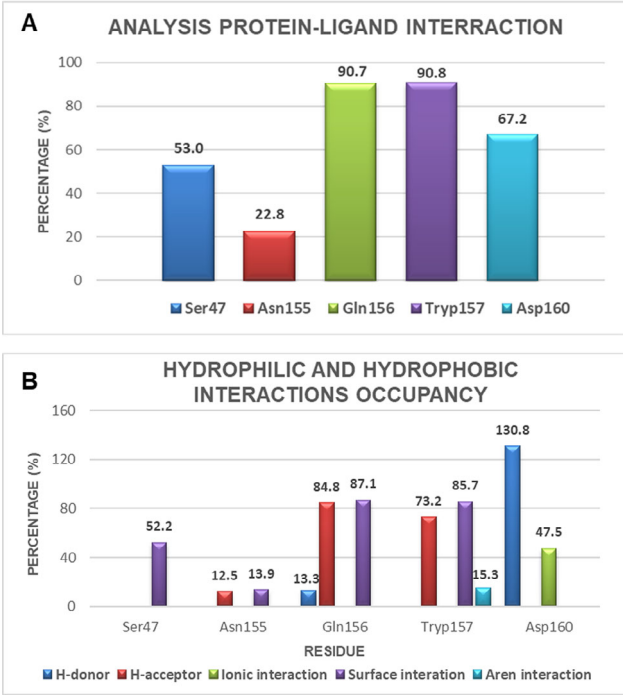

Figure 4. Frequency interaction between ligands and critical residues at the binding pocket. (A) Analysis of protein-ligand interaction occupancy and (B) Hydrophilic and hydrophobic interactions occupancy.

Table 2. The RMSD, RMSF, SASA, and Rg values of 11 complexes and protein during 50 ns MD simulation.

Complex	RMSD (nm)	RMSF (nm)	SASA (nm^2)	Rg (nm)
Apo-IL6	0.19 ± 0.03	0.10 ± 0.06	98.06 ± 0.93	1.49 ± 0.02
DB00619	0.18 ± 0.03	0.09 ± 0.06	97.77 ± 0.95	1.49 ± 0.01
DB06190	0.19 ± 0.03	0.10 ± 0.06	97.92 ± 0.92	1.49 ± 0.01
DB07601	0.21 ± 0.03	0.10 ± 0.06	98.12 ± 0.89	1.49 ± 0.01
DB09079	0.19 ± 0.03	0.09 ± 0.06	98.05 ± 0.83	1.49 ± 0.01
DB11526	0.18 ± 0.03	0.09 ± 0.06	97.68 ± 0.98	1.49 ± 0.01
DB04125	0.24 ± 0.06	0.10 ± 0.08	97.52 ± 0.92	1.49 ± 0.02
DB04739	0.24 ± 0.03	0.09 ± 0.07	97.40 ± 0.92	1.50 ± 0.01
DB15187	0.19 ± 0.05	0.10 ± 0.06	97.83 ± 0.91	1.49 ± 0.01
DB06364	0.21 ± 0.03	0.10 ± 0.07	98.82 ± 0.86	1.51 ± 0.01
DB13060	0.19 ± 0.03	0.09 ± 0.06	98.31 ± 0.88	1.50 ± 0.01
DB16236	0.27 ± 0.13	0.14 ± 0.09	98.79 ± 0.86	1.48 ± 0.02

in the MOE suite. The results showed that the key residues of IL-6 such as Gln156, Tryp157, and Asp160 could form different hydrophilic and hydrophobic interactions with ligands at a high rate of 90.7%, 90.8%, and 67.2%, respectively (Figure 4).

Regarding hydrophilic interaction, Asp160 had the highest contribution of the total poses, forming a salt bridge and hydrogen bond donor with a frequency of 47.5% and 130.8%, respectively. While, Gln156 and Tryp157 served as hydrogen acceptors with a frequency of 84.8%, and 73.2%, respectively. Besides, the ligands could also form hydrophobic interactions, including surface contacts and arene-arene interactions. In which surface contact was much more dominant, with the occupancy percentage in two vital residues of 87.1% (Gln156) and 85.7% (Tryp157). In brief, the PLIF results elucidated the chemical interactions between the critical residues of IL-6 and ligands. Based on the docking score and interaction analysis, 11 potential candidates were selected to be further tested in the next step. Detailed information about ligand-protein interaction models of these structures can be found in Table 1 and Figure S1.

Molecular dynamics simulation

The top 11 ligands from the docking step were MD simulated in 50 ns to be confirmed stability over time. These short MD trajectories were used to analyze the stability of protein, ligands, their interactions and binding free energy, after which the most potential candidates can be selected for longer MD simulations. The average values of every parameter calculated from molecular dynamics (MD) trajectories are shown in Table 2. Both LFP (apoprotein) and the LBPs had average RMSD values are less than 0.3 nm, so the stability of these ligands is accepted (Maiorov & Crippen, 1994). There were six ligands, namely DB00619, DB06190, DB09079, DB11526, DB15187, and DB13060, induced the stability of the protein, with the RMSD values in the complexes lower than IL-6 apoprotein (0.19 ± 0.03 nm). These ligands were predicted to maintain protein structure when binding to IL-6. The protein backbone RMSD plotting of each complex was illustrated separately in Figure S2. Most of the LBPs gained RMSD values fluctuating stably under 0.1 nm during the simulated time, except for DB16236.

The flexibility levels of residues in the binding site were evaluated via RMSF value. The RMSF graph of IL-6 protein in each complex is shown in Figure S3, in which most of the residue except the loop gained an RMSF value less than

0.2 nm, meaning a stable structure. The average RMSF values of different complexes are mentioned in Table 2. Despite DB16236, the RMSF values of IL-6 in other complexes were under that of apo-protein (0.10 ± 0.06 nm), meaning the stable interaction between ligands and IL-6 in the binding pocket over time.

The solvent-accessible surface area (SASA) is strongly correlated with protein volume, where a lower SASA profile specifies the condensed nature of the protein. In this study, the protein-ligand system's SASA parameter is calculated for each protein-ligand system and plotted in picoseconds during the simulated time. Table 2 and Figure S4 show that the average SASA values of DB07601, DB06364, DB13060, and DB11526 in the complexes with IL-6 were higher than the SASA value of apo-protein (98.06 ± 0.93 nm^2), and these binding cause significant changes in the protein structure.

The parameter radius of gyration (Rg) shows information about the compactness of the protein. A more compact protein indicates that the drug molecule has not significantly interfered with the folding mechanism of the protein. The higher levels of the average Rg values from the complexes with DB04739, DB06364, and DB13060 compared with the apoprotein (1.49 ± 0.02 nm) could identify instability and lose packing of proteins during simulation (Table 2). While other complexes had a comparatively lower average Rg value, revealing a more rigid nature, and no significant deviations are found in their structures. The Rg plotting of each complex has been depicted in Figure S5.

The hydrogen bond plays a vital role to provide a solid base for the evaluation of drug-biological macromolecule interactions. Therefore, the simulation trajectories are used for hydrogen bond calculation (Figure 5A). Their mean values in Table S2 indicate that these above-mentioned eleven complexes have a high hydrogen bond number and interact strongly with the protein. Besides, hydrogen bond occupancy between ligands and crucial residues of IL-6 were also investigated (Table S2). The H-bond occupation of > 75% was defined as a strong hydrogen bond and ≥ 50% was a medium one (Rungrotmongkol et al., 2010). Except for DB07601, most of the remaining ligands could form hydrogen bonds with at least three critical residues with moderate to high proportion. DB06190, DB09079, and DB15187, which gained a high frequency of total hydrogen bond occupation, are considered to have the strongest potential for interaction with IL-6 protein (Figure 5B).

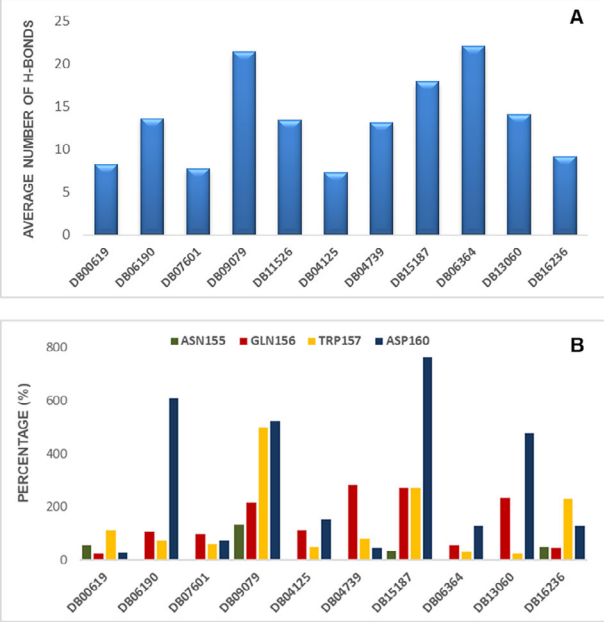

Figure 5. The hydrogen bond analysis. (A) The average number of H-bonds of eleven investigated compounds. (B) The H-bond frequency of ten ligands by residues with a frequency greater than 50%.

ADME/T screening

Small-molecule inhibitor discovery and development can be challenging due to the bioavailable effects of oral administration. Selecting appropriate candidates with a good balance of potency along with high absorption is an urgent scientific need. In this study, the drug likeliness properties of the final 11 compounds were calculated by using the SwissADME online tool and ADMET predictor 10.3 software. The ADME/T result includes physiochemical properties, medical chemistry properties, pharmacokinetics, and toxicity studies.

Physicochemical properties

Physicochemical and solubility descriptors for the top ligands are shown in Table 3. Molecular weight varied between 390 and 582 g/mol, which falls within the optimum range (200–600 g/mol) for drug-likeness. Except for DB06364, all remaining substances have no more than ten rotatable bonds, have H-bond acceptors (HDA) and H-bond donors (HDB) less than 5. The TPSA value of DB04125 is out of range standard (>140 Å). For LogP and LogS values, all compounds in our list conform to the requirements.

Medicinal chemistry properties (drug-likeness)

The estimation of drug-likeliness was done for these compounds by applying four established methods such as Lipinski's rule of 5, Veber's rule, Egan's rule, and Muegge's rule. Although most substrates meet the drug-like criteria, several of the compounds, namely DB06364, DB13060, and DB04125, could not have good oral availability because they violate one of the four rules above. Besides, two additional pattern recognition methods that allow the identification of potentially problematic fragments including PAINS and Brenk are also predicted in this study. PAINS are molecules containing substructures that exhibit potent responses in assays irrespective of the protein target and yield false-positive biological results. Brenk et al. identified 105 fragments that were evaluated to be potentially toxic, chemically reactive, metabolically unstable, or have poor pharmacokinetic properties. By applying these filters, the study will identify suitable molecular structures for the later optimization stage. Especially, one of the important aspects of screening the medicinal chemistry properties of drugs is the selection of the most promising virtual molecules for synthesis and submission for biological assays. Synthetic accessibility (SA) is a significant factor to consider in this selection process, in

Table 3. ADME/T evaluation of the 11 investigated compounds using SwissADME and ADMET Predictor® 10.3.

Properties/Compound	DB00619	DB06364	DB11526	DB15187	DB06190	DB04739	DB09079	DB16236	DB13060	DB07601	DB04125
Physicochemical											
MW	495.62	592.73	500.66	518.07	410.89	481.59	541.64	451.56	582.14	390.84	508.61
HB	4	2	3	5	3	4	4	4	5	5	5
HBD	4	8	4	4	3	4	4	2	6	4	3
NRB	8	13	8	8	8	9	9	7	10	5	9
TPSA	88.68	154.58	104.03	104.48	89	88.68	96.62	92.19	117.28	92.19	146.78
LogS	−5.08	−5.76	−5.58	−5.38	−3.4	−4.78	−5.03	−3.66	−6.02	−4.19	−4.59
LogP	1.34	2.33	1.97	1.08	2.19	0.95	0.93	1.44	1.57	1.63	1.52
Medicinal Chemistry											
PAINS	0	0	0	0	0	0	0	0	0	0	0
Brenk	0	1	0	0	0	0	0	0	0	0	1
Lipinski	Yes	No	Yes	Yes	Yes	Yes	Yes	Yes	No	Yes	Yes
Veber	Yes	No	Yes	Yes	Yes	Yes	Yes	Yes	Yes	Yes	No
Egan	Yes	No	Yes	Yes	Yes	Yes	Yes	Yes	Yes	Yes	No
Muegge	Yes	No	Yes	Yes	Yes	Yes	Yes	Yes	Yes	Yes	Yes
SA score	4.57(easy)	3.89(easy)	4.79(easy)	4.67(easy)	3.24(easy)	4.43(easy)	5.04	3.13(easy)	5.31	3.29(easy)	4.05(easy)
Pharmacokinetic											
Bioavailability Score	0.55	0.17	0.55	0.55	0.55	0.55	0.55	0.55	0.17	0.55	0.55
GI absorption	High	Low	High	High	High	High	High	High	High	High	Low
Pgp-substrate	Yes	No	Yes	Yes	Yes	Yes	Yes	Yes	No	Yes	Yes
BBB permeant	No	No	No	No	No	No	No	No	No	No	No
CYP1A2 inhibitor	No	No	No	No	No	No	No	No	No	Yes	No
CYP2C19 inhibitor	No	No	No	No	No	No	No	No	No	No	No
CYP2C9 inhibitor	No	No	Yes	No	No	No	Yes	No	No	Yes	No
CYP2D6 inhibitor	No	No	No	No	No	No	No	No	No	No	No
CYP3A4 inhibitor	No	No	No	No	No	No	No	Yes	No	No	Yes
Toxic_Risk	1.67	2.00	1.87	1.00	0.00	1.50	0.50	0.50	1.50	1.00	0.34

Abbreviations: MW (molecular weight), NRB (number of the rotatable bonds), HBA (hydrogen bond acceptor), HBD (hydrogen bond donor), TPSA (topological surface area), SA score (Synthetic accessibility score), GI absorption (Gastrointestinal absorption), and BBB permeant (Blood-Brain Barrier permeant).

which the SA score ranges from 1 (easy) to 10 (difficult). Interestingly, except for DB13060 and DB09079, all ligands remaining show easy synthesis, consequently reducing the cost and time to make these compounds in the laboratory. All results of medicinal chemistry properties from SwissADME software can be seen in Table 3.

Pharmacokinetic properties

The SwissADME prediction demonstrated that most of the ligands have a high GI absorption towards the human body and have a moderate bioavailability score of 0.55 except for DB06364 and DB04125. However, these ligands are predicted to act as a substrate of P-gp, suggesting that they can be decreased intestinal absorption. On the other hand, the impermeability of the blood-brain barrier is considered a pharmacokinetic advantage of all ligands above. As such they do not cause central nervous system depression or drowsiness as side effects. The final two SwissADME predictions for the top ten ligands focused on inhibiting of the five major cytochromes P450 isoforms (CYP1A2, CYP2C19, CYP2C9, CYP2D6, CYP3A4) and the toxic_risk prediction. According to the provided data in Table 3, all ten of the best ligands have a toxic_risk score smaller than 2, which means that these ligands were predicted as non-toxicants. For the cytochrome P450 enzymes, inhibition of these isoenzymes is undoubtedly one major cause of pharmacokinetics-related drug-drug interactions leading to toxic or other unwanted adverse effects due to the lower clearance and accumulation of the drug or its metabolites. From the data provided in Table 3, it could be seen that most of the ligands were not inhibitors of the above-mentioned metabolic enzymes.

Finally, based on the 50 ns MD simulation results and ADME/T predictions, we select the potential compounds for the next step. Specifically, the chosen ligands must meet the following criteria: (1) the fluctuations of RMSD, RMSF, SASA, and Rg are less than 0.2 nm and their mean values are less than that of apo-IL6, respectively; (2) the frequency of hydrogen bonding with residues of IL-6 must be greater than 50%; (3) the ligands must follow Lipinski, Vebber, Egan, and Muggue's rules, have no PAINs and Brenk warnings, be well absorbed orally, have no severe toxicity, and be easy to synthesize. From there, the 200 ns MD simulation is conceived and analyzed to investigate further the binding processes of these peak compounds, including DB00619, DB06190, and DB15187.

Identify the top hit compounds by 200 ns MD simulation

Similar to the 50 ns MD simulations, RMSD, RMSF, SASA, and Rg profiles are also used to evaluate protein stability in three complexes. As observed in Figure 6A, both the apoprotein and the complexes have protein backbone RMSD values fluctuating under 0.2 nm. However, the RMSD of IL-6/DB06190 has a higher volatility than the other two complexes. For the apo-IL6, except for the strong fluctuations between the 100 ns and 120 ns intervals, the protein reached equilibrium from about the first ten ns and remained stable throughout the simulation. For complexes, the RMSD of the IL-6/DB15187 and IL-6/DB00619 complexes also stabilized early after the first ten ns with the mean values $<$ 0.3 nm except for a high fluctuation at around 80 ns to 120 ns. By contrast, the RMSD of IL-6/DB06190 increased to over 0.4 nm and

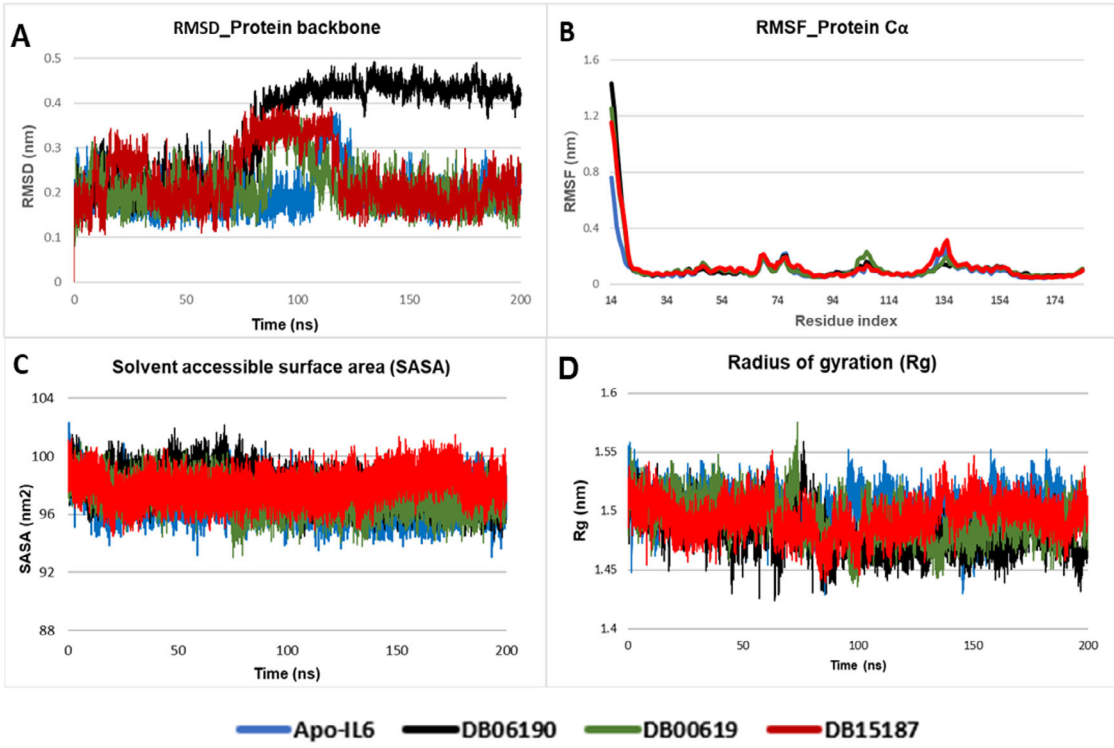

Figure 6. Analysis of RMSD, RMSF, SASA, and Rg of IL-6 and top 3 hit compounds in the 200 ns MD simulations. (A) RMSD values of the protein backbone, (B) RMSF values of protein Cα, (C) Radius of gyration (Rg), and (D) Solvent accessible surface area (SASA).

Table 4. Percentage occupancy of ionic interactions, arene interactions, and surface contacts formed between the IL6 and the two top hit compounds were calculated by PLIF using extracted frames from trajectories of 200 ns MD simulations.

	Ionic interactions		Arene interactions		Surface contacts	
Compounds	Residues	Occupancy (%)	Residues	Occupancy (%)	Residues	Occupancy (%)
DB15187	Asp160	74%	Trp157	14%	Asp160	28.5%
	Glu106	11%	Ser47	11%	Trp157	38.5%
			Asn48	10%	Gln156	30%
					Asn155	17.5%
					Asn60	11%
					Ser47	24%
					Asn48	26.5%
DB00619	Asp160	54%	Gln156	5.5%	Asp160	20.5%
					Trp157	34%
					Gln156	18%
					Asn155	5%
					Ala153	6%

fluctuated at this level until the end of the simulation. Regarding RMSF plotting, most residues of the protein in different complexes fluctuated stably under 0.2 nm (Figure 6B). These results are in perfect agreement with SASA and Rg parameters. The Solvent Accessible Surface Area (SASA) analysis revealed no significant differences were observed in the SASA profiles of apoprotein-IL-6 and its complexes. (Figure 6C). Simultaneously, during MDs, the Radius of gyration (Rg) graph shows no significant fluctuations observed by both apoprotein and complex forms (Figure 6D). Regarding the hydrogen occupancy, DB06190 has an extremely low frequency of hydrogen occupancy with critical residues, this ligand almost lost its interaction at the IL-6 binding pocket (Table S3). Based on the MD results, DB00619 and DB15187 were selected for further analysis and evaluation steps of this study.

Protein-ligand contacts analyses during 200 ns MD simulation

Interaction between protein and ligand during 200 ns was analyzed using a PLIF study of 200 frames extracted from MD trajectories. We conducted a detailed analysis of the protein-ligand contacts for the top 2 hits, DB15187 and DB00619. The findings showed that these two ligands maintain hydrogen bonding, hydrophobic, arene, and salt bridge (ionic) interactions with the critical residues of IL-6 (Asn155, Gln156, Trp157, and Asp160) throughout the MD simulation period (Table 4 and Table S3).

In particular, the binding mode of DB15187 in Figure 7A clearly shows that the highest H-bond occupancy was recorded on Asp160, Gln156, and Trp157 residues with a value of 191%, 66%, and 52%, respectively. The Asp160 and Gln156

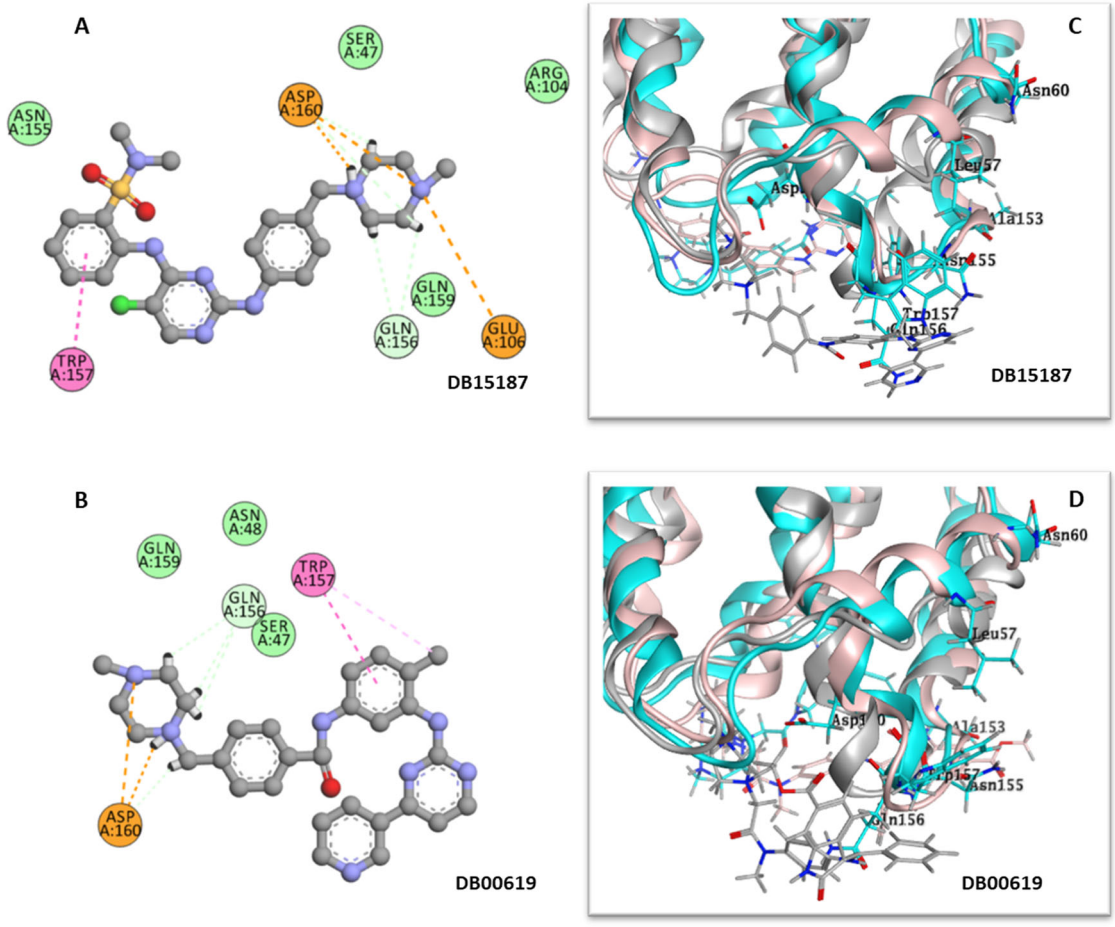

Figure 7. The detailed interaction diagram of the ligand atoms with the IL-6 critical residues. (A) and (B) The protein-ligands complexes' 2D binding mode, (C) and (D) The overlapping images of the complexes of IL-6 with ligands, at the time points 0 (in gray), 100 (in pink), and 200 ns (in cyan) of MD simulations, respectively.

Table 5. The calculation of binding free energy results in 2 top hit ligands.

Complex	ΔE_{VDW} (kcal/mol)	ΔE_{ELE} (kcal/mol)	ΔE_{GAS} (kcal/mol)	ΔE_{GB} (kcal/mol)	ΔE_{SA} (kcal/mol)	ΔE_{SOL} (kcal/mol)	ΔE_{BIND} (kcal/mol)
DB15187	−24.03 ± 2.09	−201.49 ± 15.14	−225.52 ± 15.65	206.80 ± 14.72	−3.92 ± 0.18	202.89 ± 15.65	**−22.63 ± 2.87**
DB00619	−20.44 ± 5.06	−176.00 ± 36.02	−196.44 ± 33.26	182.34 ± 32.26	−3.25 ± 0.22	179.09 ± 32.34	**−17.35 ± 2.56**

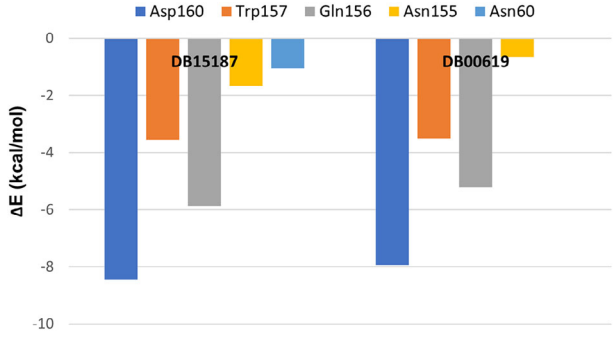

Figure 8. Contribution energy of critical residues in establishing different interactions with DB15187 and DB00619.

residues interact as HBA with ligand through side chain while Trp157 interacts as HBD using backbone (Table S3). In addition, Asp 160 also forms strong salt bridge interactions with the aromatic amines of the ligand with a high frequency of 74% (Table 4). For the hydrophobic interaction, the conjugated aromatic ring system of Trp157 forms edge-to-face contact with DB15187 by Pi-alkyl and arene-arene stacking with a total frequency of 38.5% and 14.0%, respectively. Asn155 and Gln156 participated in surface interaction with the aromatic rings of ligand using their sidechain and backbone with a total frequency of 17.6% and 30.0%, respectively (Table 4).

From Figure 7B, Table S3, and Table 4, it can be seen that DB00619 also forms interactions with the critical residues similar to DB15187 but with a lower frequency. The most prominent is the contact between Asp160 and the ligand; this residue form hydrogen bonds and salt-bridge interactions with DB00619 with a total high frequency of 143% and 54%, respectively. When the H-bond occupancy exceeds 50%, the H-bond could remain stable. Therefore, Asp160 is considered to play a vital role in the forming of stable IL-6/DB00619 complex structures through hydrogen bonds and salt bridge interactions.

Furthermore, the images of IL-6/DB15187 and IL-6/DB00619 at the binding pocket at 0 ns, 100 ns, and 200 ns are also extracted to further evaluate the stable binding of the ligands to the protein (Figure 7C and D). As we expected, the ligands maintain a stable interaction at the binding cavity until the end of the simulation.

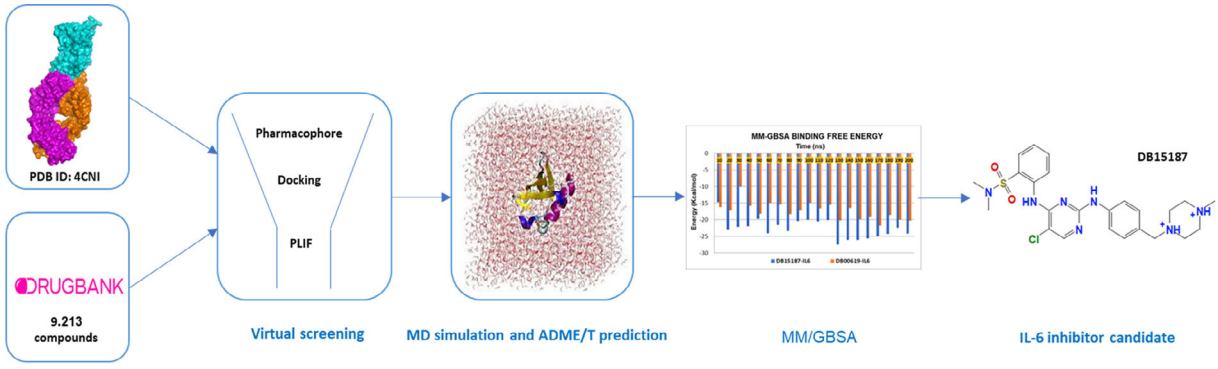

Figure 9. Summarize the studied results.

MM/GBSA

To assess the binding affinity of the IL-6/DB15187 and IL-6/DB00619 over time, the study conducted a sequential protocol of MM/GBSA protein-ligand binding energy calculations based on MD trajectories. Binding free energies between IL6 and the 2 selected ligands were calculated based on data from 2001 frames of the 200 ns MD trajectories (from frame 1 to 20001 with the interval of 10). The ΔE_{bind} allows the estimation of the affinity of a compound for a target protein; at more negative values, the compounds are more affine for the protein. As seen in Figure S6 and Table 5, the absolute binding free energy (ΔE_{bind}) of a complex was calculated as the sum of gas-phase energy (ΔE_{GAS}) and solvation free energy (ΔE_{SOL}). With the highest mean binding energy of -22.63 ± 2.87 kcal/mol, DB15187 was considered to gain a strong binding affinity with IL-6 protein over time.

Additionally, per-residue energy decomposition over the same time intervals is performed to determine the contribution of the critical residues in the interaction with the ligands more clearly. The results are described in Table S4 and Figure 8. As analyzed above, DB15187 and DB00619 interacted mainly via hydrogen bonds and salt bridge interactions with the vital residue Asp160, leading to significant free energy levels of -8.46 and -7.93 kcal/mol, respectively. In addition, Gln156 contributed to DB15187 and DB00619's total binding affinity with free energies of -5.87 and -5.21 kcal/mol, respectively. Similarly, Trp157 also contributed to a part of the energy with values of -3.56 and -3.52 kcal/mol, respectively. Asp160 and Trp157 are reported as parts of the active site in several previous studies (Paonessa et al., 1995) but their role in effective inhibitor binding is not discussed. The results of the present study highlight the importance of these critical residues in inhibitor recognition and binding at the IL-6 active site. Moreover, the contribution of binding free energies from individual key residues and the overall binding energy suggested that the DB15187 compound has a stronger binding affinity for IL-6 than the DB00619.

Conclusions

Protein-protein interactions involve important cellular activities and their signaling pathways. Thus it is considered a promising target for drug discovery. However, in terms of small molecule drugs, the physical nature of the protein-protein surface interactions renders them unable to support the binding of small drug-like molecules (Oláh et al., 2022; Petta et al., 2016). In recent years, significant advances in the development of biological strategies along and X-ray diffraction techniques have facilitated the discovery of small molecule PPI inhibitors (Bojadzic & Buchwald, 2018). Based on the X-ray crystal structure, hot spots on the protein-protein interaction interface between IL-6/Olokizumab were identified. They became the primary targets for the discovery of small molecule IL-6 inhibitors (Paonessa et al., 1995; Rosell & Fernández-Recio, 2018).

Following these findings, we designed a virtual screening procedure to identify potential IL-6 inhibitors suitable for further experimental studies. From the selected hits, 11 compounds presented docking scores of less than -20 kJ.mol^{-1} and showed important hydrogen bonds between these molecules and critical residues at the binding site, such as Asp160, Trp157, and Gln156. The 50 ns and 200 ns MD simulations were employed to indicate expressive conformational changes of the IL-6 structure in the presence of these compounds. Furthermore, MM-GBSA technique predicted the good value of binding free energies (ΔE_{bind}) of two candidates to IL-6. It is worth mentioning that ADME-Tox predictions were also performed to evaluate the safety profiles of the selected compounds. In summary, based on suitable computational approaches, including the stability of complexes and ligands, frequency of interactions occupancy, MM/GBSA binding free energy, and per-residues energy decomposition, we succeeded in identifying DB15187 as the most potential IL-6 inhibitor. The *in silico* process is summarized in Figure 9. The present study will help develop more anti-inflammatory drugs in the future, even against COVID-19, and provide some valuable information on understanding the molecular mechanism of IL6 inhibitors.

Disclosure statement

No potential conflict of interest was reported by the authors.

Funding

This work was supported by the VietNam National Foundation for Science and Technology Development (NAFOSTED) under the Grant Number 108.05-2018.15 (to Quoc-Thai Nguyen).

ORCID

Quoc-Thai Nguyen http://orcid.org/0000-0001-6315-2974
Van-Thanh Tran http://orcid.org/0000-0002-4976-0436
Khac-Minh Thai http://orcid.org/0000-0002-5279-9614

References

Akbari, M., & Hassan-Zadeh, V. (2018). IL-6 signalling pathways and the development of type 2 diabetes. *Inflammopharmacology*, *26*(3), 685–698. https://doi.org/10.1007/s10787-018-0458-0

Allegra, A., Penna, G., Alonci, A., Russo, S., Greve, B., Innao, V., Minardi, V., & Musolino, C. (2013). Monoclonal antibodies: potential new therapeutic treatment against multiple myeloma. *European Journal of Haematology*, *90*(6), 441–468. https://doi.org/10.1111/ejh.12107

Allen, S. J., & Lumb, K. J. (2020). Chapter Ten - Protein-protein interactions: a structural view of inhibition strategies and the IL-23/IL-17 axis. In R. Donev (Ed.), *Advances in protein chemistry and structural biology* (pp. 253–303). Academic Press.

Azevedo, A., Cunha, V., Teixeira, A. L., & Medeiros, R. (2011). IL-6/IL-6R as a potential key signaling pathway in prostate cancer development. *World Journal of Clinical Oncology*, *2*(12), 384–396. https://doi.org/10.5306/wjco.v2.i12.384

Bojadzic, D., & Buchwald, P. (2018). Toward small-molecule inhibition of protein-protein interactions: general aspects and recent progress in targeting costimulatory and coinhibitory (immune checkpoint) interactions. *Current Topics in Medicinal Chemistry*, *18*(8), 674–699. https://doi.org/10.2174/1568026618666180531092503

Boulanger, M. J., Chow, D-c., Brevnova, E. E., & Garcia, K. C. (2003). Hexameric structure and assembly of the interleukin-6/IL-6 alpha-receptor/gp130 complex. *Science (New York, NY)*, *300*(5628), 2101–2104. https://doi.org/10.1126/science.1083901

Brooks, B. R., Brooks, C. L., 3rd, Mackerell, A. D., Jr., Nilsson, L., Petrella, R. J., Roux, B., Won, Y., Archontis, G., Bartels, C., Boresch, S., Caflisch, A., Caves, L., Cui, Q., Dinner, A. R., Feig, M., Fischer, S., Gao, J., Hodoscek, M., Im, W., Kuczera, K., Lazaridis, T., Ma, J., Ovchinnikov, V., Paci, E., Pastor, R. W., Post, C. B., Pu, J. Z., Schaefer, M., Tidor, B., Venable, R. M., Woodcock, H. L., Wu, X., Yang, W., York, D. M., … Karplus, M. (2009). CHARMM: the biomolecular simulation program. *Journal of Computational Chemistry*, *30*(10), 1545–1614. https://doi.org/10.1002/jcc.21287

Case, D. A., Cheatham, T. E., Darden, T., Gohlke, H., Luo, R., Merz, K. M., Onufriev, A., SiMMerling, C., Wang, B., & Woods, R. J. (2005). The Amber biomolecular simulation programs. *Journal of Computational Chemistry*, *26*(16), 1668–1688. https://doi.org/10.1002/jcc.20290

Castelli, M. S., McGonigle, P., & Hornby, P. J. (2019). The pharmacology and therapeutic applications of monoclonal antibodies. *Pharmacology Research & Perspectives*, *7*(6), e00535. https://doi.org/10.1002/prp2.535

Choi, J. M., Rotimi, O. O., O'Carroll, S. J., & Nicholson, L. F. (2016). IL-6 stimulates a concentration-dependent increase in MCP-1 in immortalised human brain endothelial cells. *F1000Research*, *5*, 270. https://doi.org/10.12688/f1000research.8153.2

Daina, A., Michielin, O., & Zoete, V. (2017). SwissADME: a free web tool to evaluate pharmacokinetics, drug-likeness and medicinal chemistry friendliness of small molecules. *Scientific Reports*, *7*, 42717. https://doi.org/10.1038/srep42717

Eto, D., Lao, C., DiToro, D., Barnett, B., Escobar, T. C., Kageyama, R., Yusuf, I., & Crotty, S. (2011). IL-21 and IL-6 are critical for different aspects of B cell immunity and redundantly induce optimal follicular helper CD4 T Cell (Tfh) differentiation. *PLoS One*, *6*(3), e17739. https://doi.org/10.1371/journal.pone.0017739

Genheden, S., & Ryde, U. (2015). The MM/PBSA and MM/GBSA methods to estimate ligand-binding affinities. *Expert Opinion on Drug Discovery*, *10*(5), 449–461. https://doi.org/10.1517/17460441.2015.1032936

GROMACS. (2021). Manual (Release 2021.02). Retrieved April 30, 2022, from https://doi.org/10.5281/zenodo.4457591

Hanwell, M. D., Curtis, D. E., Lonie, D. C., Vandermeersch, T., Zurek, E., & Hutchison, G. R. (2012). Avogadro: an advanced semantic chemical editor, visualization, and analysis platform. *Journal of Cheminformatics*, *4*(1), 17. https://doi.org/10.1186/1758-2946-4-17

Hirano, T. (2021). IL-6 in inflammation, autoimmunity and cancer. *International Immunology*, *33*(3), 127–148. https://doi.org/10.1093/intimm/dxaa078

Humphrey, W., Dalke, A., & Schulten, K. (1996). VMD: visual molecular dynamics. *Journal of Molecular Graphics*, *14*(1), 33–38. https://doi.org/10.1016/0263-7855(96)00018-5

Karkhur, S., Hasanreisoglu, M., Vigil, E., Halim, M. S., Hassan, M., Plaza, C., Nguyen, N. V., Afridi, R., Tran, A. T., Do, D. V., Sepah, Y. J., & Nguyen, Q. D. (2019). Interleukin-6 inhibition in the management of non-infectious uveitis and beyond. *Journal of Ophthalmic Inflammation and Infection*, *9*(1), 17. https://doi.org/10.1186/s12348-019-0182-y

Kontoyianni, M., McClellan, L. M., & Sokol, G. S. (2004). Evaluation of docking performance: comparative data on docking algorithms. *Journal of Medicinal Chemistry*, *47*(3), 558–565. https://doi.org/10.1021/jm0302997

Kuhn, K. A., Manieri, N. A., Liu, T.-C., & Stappenbeck, T. S. (2014). IL-6 stimulates intestinal epithelial proliferation and repair after injury. *PLoS One*, *9*(12), e114195. https://doi.org/10.1371/journal.pone.0114195

Lacroix, M., Rousseau, F., Guilhot, F., Malinge, P., Magistrelli, G., Herren, S., Jones, S. A., Jones, G. W., Scheller, J., Lissilaa, R., Kosco-Vilbois, M., Johnson, Z., Buatois, V., & Ferlin, W. (2015). Novel insights into interleukin 6 (IL-6) Cis- and trans-signaling pathways by differentially manipulating the assembly of the IL-6 signaling complex. *The Journal of Biological Chemistry*, *290*(45), 26943–26953. https://doi.org/10.1074/jbc.M115.682138

Le, M. T., Hoang, V. N., Nguyen, D. N., Bui, T. H. L., Phan, T. V., Huynh, P. N. H., Tran, T. D., & Thai, K. M. (2021). Structure-based discovery of ABCG2 inhibitors: A homology protein-based pharmacophore modeling and molecular docking approach. *Molecules*, *26*(11), 3115. https://doi.org/10.3390/molecules26113115

Le, M. T., Mai, T. T., Huynh, P. N. H., Tran, T. D., Thai, K. M., & Nguyen, Q. T. (2020). Structure-based discovery of interleukin-33 inhibitors: a pharmacophore modelling, molecular docking, and molecular dynamics simulation approach. *SAR and QSAR in Environmental Research*, *31*(12), 883–904. https://doi.org/10.1080/1062936X.2020.1837239

LeadIT 2.1.8. (2022). Version 2.1.8 [software]. Retrieved February 20, 2022, from www.biosolveit.de/LeadIT.

Maiorov, V. N., & Crippen, G. M. (1994). Significance of root-mean-square deviation in comparing three-dimensional structures of globular proteins. *Journal of Molecular Biology*, *235*(2), 625–634. https://doi.org/10.1006/jmbi.1994.1017

Molecular Operating Environment (MOE). (2015). Retrieved January 14, 2022, from https://www.chemcomp.com/Research-MOE_Citations.htm?year=2015.

Ngo, T. D., Tran, T. D., Le, M. T., & Thai, K. M. (2016). Computational predictive models for P-glycoprotein inhibition of in-house chalcone derivatives and drug-bank compounds. *Molecular Diversity*, *20*(4), 945–961. https://doi.org/10.1007/s11030-016-9688-5

Oláh, J., Szénási, T., Lehotzky, A., Norris, V., & Ovádi, J. (2022). Challenges in discovering drugs that target the protein-protein interactions of disordered proteins. *International Journal of Molecular Sciences*, *23*(3), 1550. https://doi.org/10.3390/ijms23031550

Paonessa, G., Graziani, R., De Serio, A., Savino, R., Ciapponi, L., Lahm, A., Salvati, A. L., Toniatti, C., & Ciliberto, G. (1995). Two distinct and independent sites on IL-6 trigger gp 130 dimer formation and signalling. *The EMBO Journal*, *14*(9), 1942–1951. https://doi.org/10.1002/j.1460-2075.1995.tb07186.x

Petta, I., Lievens, S., Libert, C., Tavernier, J., & De Bosscher, K. (2016). Modulation of protein–protein interactions for the development of novel therapeutics. *Molecular Therapy: The Journal of the American*

Society of Gene Therapy, *24*(4), 707–718. https://doi.org/10.1038/mt.2015.214

Potere, N., Batticciotto, A., Vecchié, A., Porreca, E., Cappelli, A., Abbate, A., Dentali, F., & Bonaventura, A. (2021). *The role of IL-6 and IL-6 blockade in COVID-19, Vol. 17, Expert. Rev. Clin. Immunol.* Taylor & Francis.

Pullamsetti, S. S., Seeger, W., & Savai, R. (2018). Classical IL-6 signaling: a promising therapeutic target for pulmonary arterial hypertension. *The Journal of Clinical Investigation*, *128*(5), 1720–1723. https://doi.org/10.1172/jci120415

Rose-John, S., Winthrop, K., & Calabrese, L. (2017). The role of IL-6 in host defence against infections: immunobiology and clinical implications. *Nature Reviews. Rheumatology*, *13*(7), 399–409. https://doi.org/10.1038/nrrheum.2017.83

Rosell, M., & Fernández-Recio, J. (2018). *Hot-spot analysis for drug discovery targeting protein-protein interactions, Vol. 13, Expert. Opin. Drug. Discov*. Taylor & Francis.

Rungrotmongkol, T., Nunthaboot, N., Malaisree, M., Kaiyawet, N., Yotmanee, P., Meeprasert, A., & Hannongbua, S. (2010). Molecular insight into the specific binding of ADP-ribose to the nsP3 macro domains of chikungunya and Venezuelan equine encephalitis viruses: molecular dynamics simulations and free energy calculations. *Journal of Molecular Graphics & Modelling*, *29*(3), 347–353. https://doi.org/10.1016/j.jmgm.2010.09.010

Sekhar Pagadala, N. (2021). Computational prediction of hERG blockers using homology modelling, molecular docking and QuaSAR studies. *Results in Chemistry*, *3*, 100101. https://doi.org/10.1016/j.rechem.2021.100101

Shaw, S., Bourne, T., Meier, C., Carrington, B., Gelinas, R., Henry, A., Popplewell, A., ADAms, R., Baker, T., Rapecki, S., Marshall, D., Moore, A., Neale, H., & Lawson, A. (2014). Discovery and characterization of olokizumab: a humanized antibody targeting interleukin-6 and neutralizing gp130-signaling. *MAbs*, *6*(3), 774–782. https://doi.org/10.4161/mabs.28612

Simulations Plus. (2022). "ADMET Predictor®." Version 10.3. Retrieved August 10, 2022, from https://www.simulations-plus.com/software/admetpredictor/

Thai, K. M., Ngo, T. D., Tran, T. D., & Le, M. T. (2013). Pharmacophore modeling for antitargets. *Current Topics in Medicinal Chemistry*, *13*(9), 1002–1014. https://doi.org/10.2174/1568026611313090004

The Protein Data Bank. (2022). Retrieved January 4, 2022, from https://www.rcsb.org/structure/4CNI

Tran, Q. H., Nguyen, Q. T., Vo, N. Q., Mai, T. T., Tran, T. T., Tran, T. D., Le, M. T., Trinh, D. T., & Thai, K. M. (2022). Structure-based 3D-Pharmacophore modeling to discover novel interleukin 6 inhibitors: An in silico screening, molecular dynamics simulations and binding free energy calculations. *PLoS One*, *17*(4), e0266632. https://doi.org/10.1371/journal.pone.0266632

Tran, T. T. N., Tran, Q. H., Nguyen, Q. T., Le, M. T., Trinh, D. T. T., Tran, V. H., & Thai, K. M. (2022). LY3041658/interleukin-8 complex structure as targets for IL-8 small molecule inhibitors discovery using a combination of in silico methods. *SAR and QSAR in Environmental Research*, *33*(10), 753–778. https://doi.org/10.1080/1062936X.2022.2132536

Tran, T. T. N., Tran, Q. H., Nguyen, Q. T., Le, M. T., Trinh, D. T. T., & Thai, K. M. (2022). Identification of potential interleukin-8 inhibitors acting on the interactive site between chemokine and CXCR2 receptor: A computational approach. *PLoS One*, *17*(2), e0264385. https://doi.org/10.1371/journal.pone.0264385

Valdés-Tresanco, M. S., Valdés-Tresanco, M. E., Valiente, P. A., & Moreno, E. (2021). gmx_MMPBSA: A new tool to perform end-state free energy calculations with GROMACS. *Journal of Chemical Theory and Computation*, *17*(10), 6281–6291. https://doi.org/10.1021/acs.jctc.1c00645

Verma, R., Yadav, M., Pradhan, D., Bhuyan, R., Aggarwal, S., Nayek, A., & Jain, A. K. (2016). Probing binding mechanism of interleukin-6 and olokizumab: in silico design of potential lead antibodies for autoimmune and inflammatory diseases. *Journal of Receptor and Signal Transduction Research*, *36*(6), 601–616. https://doi.org/10.3109/10799893.2016.1147584

Wang, E., Sun, H., Wang, J., Wang, Z., Liu, H., Zhang, J. Z. H., & Hou, T. (2019). End-point binding free energy calculation with MM/PBSA and MM/GBSA: Strategies and applications in drug design. *Chemical Reviews*, *119*(16), 9478–9508. https://doi.org/10.1021/acs.chemrev.9b00055

Wang, J. (2009). Comprehensive assessment of ADMET risks in drug discovery. *Current Pharmaceutical Design*, *15*(19), 2195–2219. https://doi.org/10.2174/138161209788682514

Wishart, D. S., Feunang, Y. D., Guo, A. C., Lo, E. J., Marcu, A., Grant, J. R., Sajed, T., Johnson, D., Li, C., Sayeeda, Z., Assempour, N., Iynkkaran, I., Liu, Y., Maciejewski, A., Gale, N., Wilson, A., Chin, L., Cummings, R., Le, D., … Wilson, M. (2018). DrugBank 5.0: a major update to the DrugBank database for 2018. *Nucleic Acids Research*, *46*(D1), D1074–d1082. https://doi.org/10.1093/nar/gkx1037

Zoete, V., Cuendet, M. A., Grosdidier, A., & Michielin, O. (2011). SwissParam: a fast force field generation tool for small organic molecules. *Journal of Computational Chemistry*, *32*(11), 2359–2368. https://doi.org/10.1002/jcc.21816